Spectrum-Energy-Economy Efficiency Analysis of B5G Wireless Communication Systems With Separated Indoor/Outdoor Scenarios

Yu Fu, Cheng-Xiang Wang, *Fellow, IEEE*, Xichen Mao, Jie Huang, *Member, IEEE*, Zijun Zhao, and Stephen McLaughlin, *Fellow, IEEE*

***Abstract*— In this paper, we study the spectrum efficiency (SE), energy efficiency (EE), and economic efficiency (ECE) for a heterogeneous cellular architecture that separates the indoor and outdoor scenarios for beyond 5G (B5G) wireless communication systems. For outdoor scenarios, massive multiple-input-multiple-output (MIMO) technologies and distributed antenna systems (DASs) at sub-6 GHz frequency bands are used for long-distance communications. For indoor scenarios, millimeter-wave (mmWave) and beamforming communication technologies are deployed at wireless indoor access points (IAPs) to provide high-speed short-range services to indoor users. Mathematical expressions for the system capacity, SE, EE, and ECE are derived using a proposed realistic power consumption model. The results shed light on the fact that the proposed network architecture is able to improve SE and EE by more than three times compared to those conventional network architectures. The analysis of system performance in terms of SE, EE, ECE, and their trade-off results in the observation that the proposed network architecture offers a promising solution for future B5G communication systems.**

***Index Terms*— B5G, massive-MIMO, mmWave, spectrum efficiency, energy efficiency, economy efficiency.**

Manuscript received 25 June 2022; revised 18 November 2022 and 1 March 2023; accepted 18 April 2023. Date of publication 11 May 2023; date of current version 12 December 2023. This work was supported in part by the National Key Research and Development Program of China under Grant 2021YFB2900300, in part by the National Natural Science Foundation of China (NSFC) under Grant 61960206006 and Grant 62271147, in part by the Key Technologies Research and Development Program of Jiangsu (Prospective and Key Technologies for Industry) under Grant BE2022067 and Grant BE2022067-1, in part by the High Level Innovation and Entrepreneurial Doctor Introduction Program in Jiangsu under Grant JSSCBS20210082, in part by the EU Research and Innovation Staff Exchange (RISE) project under Horizon2020 Testing and Evaluating Sophisticated Information and Communication Technologies for enaBling scalablE smart griD Deployment (TESTBED2) Project under Grant 872172, in part by the Start-Up Research Fund of Southeast University under Grant RF1028623029, in part by the Fundamental Research Funds for the Central Universities under Grant 2242023K5003, and in part by the Postgraduate Research and Practice Innovation Program of Jiangsu Province under Grant SJCX22_0042. The associate editor coordinating the review of this article and approving it for publication was S. Zhou. *(Corresponding author: Cheng-Xiang Wang.)*

Yu Fu was with the School of Engineering and Physical Sciences, Institute of Sensors, Signals and Systems, Heriot-Watt University, EH14 4AS Edinburgh, U.K. He is now with Scotia Security Group, Scotia House, EH20 9LZ Edinburgh, U.K. (e-mail: bzfy1986@gmail.com).

Cheng-Xiang Wang, Xichen Mao, and Jie Huang are with the National Mobile Communications Research Laboratory, School of Information Science and Engineering, Southeast University, Nanjing 210096, China, and also with the Purple Mountain Laboratories, Nanjing 211111, China (e-mail: chxwang@seu.edu.cn; xcmao@seu.edu.cn; j_huang@seu.edu.cn).

Zijun Zhao is with the TDD Solution Design Department, Huawei Technologies, Shanghai 201206, China (e-mail: zhaozijun3@huawei.com).

Stephen McLaughlin is with the School of Engineering and Physical Sciences, Institute of Sensors, Signals and Systems, Heriot-Watt University, EH14 4AS Edinburgh, U.K. (e-mail: s.mclaughlin@hw.ac.uk).

Color versions of one or more figures in this article are available at https://doi.org/10.1109/TWC.2023.3273261.

Digital Object Identifier 10.1109/TWC.2023.3273261

I. Introduction

WITH the widespread commercialization of fifth-generation (5G) wireless communication system, extensive research into next-generation communication systems has been conducted [1], [2]. Currently, a variety of novel technologies have been proposed for beyond 5G (B5G) systems [3] and it can be validated that these techniques will improve system performance. In particular, massive multiple-input multiple-output (MIMO) technology, which employs tens to hundreds of antennas, has attracted significant research interest in recent years [4], [5], [6]. Massive MIMO technology has shown its capability to increase the system capacity by exploiting the asymptotic orthogonal characteristic of high-dimensional random channel vectors [7], [8]. Moreover, millimeter-wave (mmWave) communication can provide a viable solution that enables Gbps-level wireless data transmission and potentially mitigate the problem of spectrum shortage in the crowded sub-6 GHz frequency bands [9], [10].

In addition to novel access technologies, significant changes in the network architecture will also play a pivotal role in boosting the system performance, e.g., by adopting distributed antenna systems (DASs), relay system, or cell-free architecture [11], [12], [13], [14]. The 5G system adopts the cellular architecture using next generation Node B (gNB) to serve both indoor and outdoor users simultaneously. However, with the surge of application scenarios, the existing architecture is unable to meet future technical requirements and the system interference remains a significant challenge for 5G [3]. Different from existing network architectures, a heterogeneous cellular architecture separating indoor and outdoor scenarios for 5G and B5G wireless communication systems was proposed in [15]. In this architecture, the outdoor user equipment (UE) were served by the base station equipped with a large antenna array and assisted with DAS, and the indoor UE were served by indoor access points (IAPs). The macro base station (MBS) ensures a homogeneous quality of service (QoS) inside the cell with massive MIMO systems that are further utilized to boost the system capacity. The IAP can provide a high-speed network access for the indoor UE by exploiting technologies such as the femtocell, WiFi, mmWave, terahertz (THz), and visible light communications. Its connection with the MBS can be established by the passive optical network, massive MIMO, mmWave technology, and even free-space optical technology. This architecture avoided the penetration loss that results from the signal passing through building walls that can be over 24 dB for buildings with energy-efficient insulating layers [15].

Due to the shortage of spectrum resource and the increase in system power consumption, spectral efficiency (SE) and energy efficiency (EE) are the two most valuable key performance indicators (KPIs). In [16], fundamental trade-offs between KPIs, including SE and EE trade-off, were proposed. As a result, in recent years, a great deal of research has been carried out on SE, EE, and their trade-offs, which considered the emerging new technologies and network architectures. SE and EE were studied in [17] and [18] with a focus on downlink MIMO and massive MIMO relay systems. In [19], the authors investigated the trade-off between SE and EE for massive MIMO technology, while a similar study considering cell-free massive MIMO systems was conducted in [20]. A study on the trade-off between SE and EE, which aimed at achieving a multi-objective-optimization, was carried out in [21]. In [22], the trade-off between SE and EE in a multi-user (MU) massive MIMO system was investigated, where the interference had the primary impact on the system performance. In [23], the authors derived the expression of SE for DAS system and investigated the effects of main parameters on the system performance. In relay wireless networks, various SE-EE trade-offs were addressed in [12], [13], [24], and [25]. In [12] and [13], SE and EE of relay-aided cellular networks were investigated. A full-duplex relay system and an amplify-and-forward relay were considered in [24] and [25], respectively. In [26] and [27], SE and EE of massive MIMO relay system employing zero-forcing were analyzed and the impact of transceiver power consumption on EE was revealed in [26]. As a key technology for 5G, small cell technology has attracted considerable research interests, and related researches concerning SE and EE in small cell scenarios can be found in [28] and [29]. In [28], metrics, methods, and market of EE for small cell network were summarized. In [29], EE of full-duplex mmWave relays with precoding was studied. In [30], EE of B5G ultra dense networks was studied, which considered a single-cell scenario using massive MIMO and visible light communication techniques.

As system complexity, operating costs, and user business volume increase, it is difficult to only utilize SE and EE to delineate system performance comprehensively. For communication operators, it is vital to analyze system performance from an economic perspective by a novel KPI. In [13], a new performance metric named the economic efficiency (ECE) was proposed as a complementary performance measure to SE and EE. In [31], the system performance in terms of SE, EE, and ECE was studied in spatial modulation based wireless system. Cost efficiency, which is very similar to ECE, of mmWave /ultra high frequency (UHF)-based cellular networks was investigated in [32].

Although the performance analysis of wireless communication systems has been widely investigated, some gaps remain.

1) Although a novel indoor and outdoor separated architecture which can reduce interference was proposed in [15], the related research on this architecture is limited. Moreover, the existing research on SE and EE of a complete communication system, especially for potential B5G systems, is limited.
2) The power consumption models used in most research are simple and not sufficiently accurate to evaluate the EE. In other works, the power consumptions only focused on base stations (BSs) [33], [34]. Additionally, most power models omit some critical components and factors. In [35], the RF components power model ignored the differences between options, while [29] neglected the impact of PA kinds.
3) The investigation of SE, EE, and ECE in most existing works only focused on one or two performance metrics. Specifically, studies on the ECE performance of B5G wireless systems are very limited.

To address the issues listed above, in this paper we investigate a B5G use case with separate indoor and outdoor cellular deployment. This system employs massive MIMO assisted DAS technology for the outdoor UE coverage and the IAP access link to the MBS, while mmWave based beamforming is used for the indoor UE access. We also investigate the SE, EE, ECE, and their related trade-offs for the proposed network architecture. The main contributions of this paper are summarized as follows.

1) The SE, EE, ECE, and their associated trade-offs for a novel B5G use case that separates the indoor and outdoor scenarios are investigated. The simulation results exemplify that the proposed network architecture could be an option for future wireless system as it can achieve better performance in terms of SE, EE, and ECE.
2) The framework for building practical power consumption models of B5G systems is developed. In particular, we consider baseband operations, RF front-end, and different types of power amplifiers. As this model can represent the details of B5G systems, this framework can be used as a guideline to accurately model, predict, and evaluate the system performance in terms of power consumption for future wireless systems.

The remainder of the paper is organized as follows. In Section II, the system model is presented. In Section III, mathematical expressions for the system capacity, SE, EE, and ECE are derived. In Section IV, the mathematical and simulation results are presented and analyzed. Finally, conclusions are drawn in Section V.

II. System Model

A typical B5G cellular architecture with the separate indoor and outdoor coverage is shown in Fig. 1. One MBS is connected to several large-scale antenna arrays geographically distributed in the cell, referred to as MBSA in this paper. Each antenna array serves a particular area where UEs are located, and also provides wireless data links for buildings in which indoor UEs are located. We assume all buildings in the cell have antenna arrays installed on the exterior walls or the roof, referred as building mounted antenna arrays (BMAA).

Inside each BMAA, IAPs are deployed to provide the wireless coverage to indoor UEs, which relay the traffic between the indoor UE and the MBS outside. Each IAP is connected

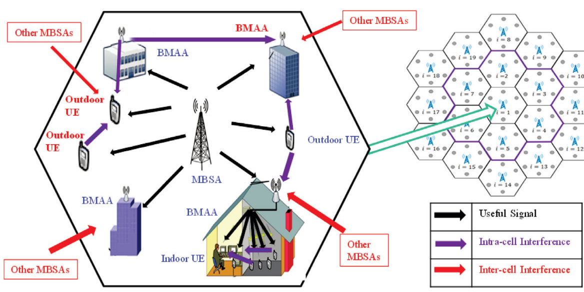

Fig. 1. The system model of a potential B5G wireless network.

to the antenna array with a fiber to avoid the significant penetration loss caused by the building walls. A BMAA communicates with a MBSA via conventional sub-6 GHz bands, and a line-of-sight (LoS) path is ensured between a BMAA and its serving MBSA. To exploit the LoS path, beamforming technologies can be utilized to create several virtual links between each pair of a MBAA and a BMAA.

For the indoor coverage, the IAP employs beamforming mmWave communication technology. By using this technology, each IAP can serve several active indoor UE simultaneously with the orthogonal beams in a high-speed and intercell-interference-free manner. Since the outdoor and indoor systems occupy different frequency bands, there is no interference between the outdoor and indoor UEs. In addition, as a result of the high penetration loss of mmWave signals, there is no interference among IAPs in different neighboring buildings.

Specifically, the whole coverage area of the MBS is separated into N_a sub-areas. Each sub-area is served by a MBSA connected to this MBS. The MBSA is equipped with M_T antenna elements, and serves N_{oue} outdoor UE plus N_b buildings within the sub-area. For each BMAA, M_R antenna elements are deployed, and there are L ensured beamforming paths to its serving MBSA. In this paper, we assume one MBSA is subject to the interference from N_{I} neighboring MBSAs which could be in the same or the neighboring cells with the index set denoted by $\mathcal{N}(i)$. BMAA is assumed to suffer from both inter-cell and intra-cell interference. An IAP is equipped with M_{Tq} antenna elements and serves N_{iue} indoor UEs each has M_{Rq} receive antenna elements. For outdoor UEs, they are assumed to have a single receive antenna. In order to compare the system performance, we consider a non-separated communication scenario as a contrast. In this condition, both the indoor and outdoor UE communicate with the outdoor MBSA directly. While in the separated communication scenario, the BMAA communicates with the MBS via the massive MIMO technology at sub-6 GHz frequency bands as the outdoor link, and the indoor users utilize some short-range and high-frequency technologies to communicate with the IAPs, such as mmWave, to make the indoor link.

A. Channel Model

For this system, there are two different communication environments, one is the outdoor environment which includes the link between the MBSA and the BMAA, and the other is the link between MBSA and outdoor UE. For the indoor environment, only the links between IAPs and the served indoor UE are considered.

1) Outdoor Channel: The outdoor massive MIMO beamforming channels can be further categorized into two types, which represent the channel between the MBSA and BMAA, and the channel between the MBSA and outdoor UE.

- The channel model of the ℓ-th beam path between the i-th MBSA and the j-th BMAA is given by

$$\boldsymbol{G}_{\ell ji} = \sqrt{\beta_{\ell ji} M_T M_R}\boldsymbol{a}^*_{M_R}(\phi_{\ell ji})\boldsymbol{a}^T_{M_T}(\theta_{\ell ji}) \tag{1}$$

where $\theta_{\ell ji}$ is the angle of departure (AoD) at the i-th MBSA, $\phi_{\ell ji}$ is the angle of arrival (AoA) of the j-th BMAA, $\beta_{\ell ji}$ is the path loss, and

$$\begin{aligned}&\boldsymbol{a}_M(\theta)\\&= \frac{1}{\sqrt{M}}[1, \ldots, e^{-\jmath 2\pi\Delta(m-1)\sin\theta}, e^{-\jmath 2\pi\Delta(M-1)\sin\theta}]^T\end{aligned} \tag{2}$$

represents the antenna response, M can be either M_R or M_T. Without loss of generality, the uniform linear array is adopted as the representative. The system model can be easily extended to other types of antenna arrays by changing the antenna response vector. The normalized antenna separation is represented as Δ, and we assume $\Delta = 1/2$ without loss of generality [36], [37]. The transmission beam vector at the BMAA is defined as $\boldsymbol{a}^*_{M_T}(\theta_{\ell ji})$, and the receiving beam vector at the BMAA is represented as $\boldsymbol{a}^T_{M_R}(\phi_{\ell ji})$. As $\theta_{\ell ji}$ and $\phi_{\ell ji}$ can be adjusted and optimized when deploying the MBSA and BMAA, the beamforming channel between MBSA and BMAA can be considered as static and known to both the transmitter (Tx) and the receiver (Rx) sides.
- For the k-th outdoor user served by the i-th MBSA, the channel is described by

$$\boldsymbol{g}_{ki} = \sqrt{\beta_{ki}}\boldsymbol{h}_{ki} \tag{3}$$

where β_{ki} is the large-scale channel gain including path loss and shadowing, and $\boldsymbol{h}_{ki}$ is a $M_T \times 1$ small-scale Rayleigh channel fading vector. Each component h_{ki} of the vector $\boldsymbol{h}_{ki}$ is an independent and identically distributed (i.i.d.) complex Gaussian random variable, with zero mean and unit variance, i.e., $h_{ki} \sim N(0, 1)$.

2) Indoor mmWave Channel: Inside the building, beamforming technology is assumed to be performed at the IAP and the UE, which gives the high directional feature of the mmWave channel. The mmWave beamforming channel gain between the IAP and the q-th indoor UE can be given as

$$\boldsymbol{g}_{uq} = \sqrt{\beta_{uq} M_{Tq} M_{Rq}}\boldsymbol{a}^*_{M_{Rq}}(\phi_{uq})\boldsymbol{a}^{\mathrm{T}}_{M_{Tq}}(\theta_{uq}). \tag{4}$$

This channel gain matrix is with a dimension of $M_{Tq} \times M_{Rq}$, where θ_{uq} is the AoD at the IAP, ϕ_{uq} is the AoA at the uq-th indoor user, β_{uq} is the path loss, and $\boldsymbol{a}^*_{M_{Rq}}(\phi_{uq})$ and $\boldsymbol{a}^{\mathrm{T}}_{M_{Tq}}(\theta_{uq})$ are the antenna responses similar to expression in (2). The indoor beamforming channel gain matrix has a similar expression to the outdoor channel between the MBSA and BMAA. However, as their path-loss model and the distribution of key parameters such as the AoD and AoA are different, their propagation features can be significantly distinguished which can dramatically impact the system performance

B. Received Signal

1) Outdoor Links: For the i-th MBSA, the transmitted signal vector $\boldsymbol{x}_i$ is a linear combination of beamformed signals to its served BMAA and the linearly precoded signals for its served outdoor UE, which can be written as

$$\boldsymbol{x}_i = \sum_{j=1}^{N_b}\sum_{\ell=1}^{L} \boldsymbol{b}_{\ell ji} s_{\ell ji} + \sum_{k=1}^{N_{\text{oue}}} \boldsymbol{w}_{ki} s_{ki}. \tag{5}$$

In (5), $s_{\ell ji}$ and s_{ki} are i.i.d. complex Gaussian random variables with zero mean and variance $P_{\ell ji}$ and P_{ki}, respectively, $\boldsymbol{b}_{\ell ji} = \boldsymbol{a}^*(\theta_{\ell ji})$ denotes the ℓ-th beamforming vector to the j-th BMAAs, and $\boldsymbol{w}_{ki}$ is the linear precoding vector for the k-th outdoor UE. In this paper, the maximum-ratio transmission (MRT) precoding is applied, resulting in $\boldsymbol{w}_{ki} = \boldsymbol{h}^*_{ki}/\sqrt{M_T}$ when perfect channel state information (CSI) is assumed to be known at the MBSA side [38].

For the j-th BMAA, its received signal over the ℓ beamforming channels is given by

$$\begin{aligned} &r_{\ell ji} \\ &= \boldsymbol{a}^T_{M_R}(\phi_{\ell ji})\left(\boldsymbol{G}_{\ell ji}\boldsymbol{x}_i + \sum_{i'\in\mathcal{N}(i)}\sum_{j'=1}^{N_b'}\sum_{\ell'=1}^{L'}\boldsymbol{G}_{\ell' j' i'}\boldsymbol{x}_{i'}\right) + n \\ &= \sqrt{\beta_{\ell ji}M_T M_R}s_{\ell ji} + \sqrt{\beta_{\ell ji}M_T M_R}\sum_{k=1}^{N_{\text{oue}}}\boldsymbol{a}^T_{M_T}(\theta_{\ell ji})\boldsymbol{w}_{ki}s_{ki} \\ &\quad + \sum_{i'\in\mathcal{N}(i)}\sum_{j'=1}^{N_b'}\sum_{\ell'=1}^{L'}\boldsymbol{a}^T_{M_R}(\phi_{\ell ji})\boldsymbol{G}_{\ell' j' i'}x_{i'} + n \end{aligned} \tag{6}$$

where $\boldsymbol{a}^T_{M_R}(\phi_{\ell ji})$ is the ℓ-th receiving beam vector of the j-th BMAA, $\boldsymbol{x}_{i'}$ is the interference signal from other MBSA with $\boldsymbol{G}_{\ell' j' i'}$ as the corresponding beamforming channel matrix, and $\boldsymbol{n}$ is the receiving Gaussian noise vector. In (6), the interference consists of two parts. One is from the signal intended to be received by the outdoor UE and the other is the interference from the neighboring MBSAs. In this system, we have assumed that the antennas are installed outside the building with guaranteed line-of-sight path, as all the buildings are fixed. Thus, ideal channel estimation can be assumed. Due to the orthogonality of transmit and receive beamforming vectors, the Rx will not be subject to the interference from the uplink signal sent from other buildings. For the k-th outdoor UE, the received signal can be given by

$$\begin{aligned} r_{ki} &= \boldsymbol{g}^T_{ki}\boldsymbol{x}_i + \sum_{i'\in\mathcal{N}(i)}\boldsymbol{g}^T_{ki'}\boldsymbol{x}_{i'} + n \\ &= \boldsymbol{g}^T_{ki}\boldsymbol{w}_{ki}s_{ki} + \sum_{j=1,j\neq k}^{N_{\text{oue}}}\boldsymbol{g}^T_{ki}\boldsymbol{w}_{ji}s_{ji} + \sum_{j=1}^{N_b}\sum_{\ell=1}^{L}\boldsymbol{g}^T_{ki}\boldsymbol{b}_{\ell ji}s_{\ell ji} \\ &\quad + \sum_{i'\in\mathcal{N}(i)}\boldsymbol{g}^T_{ki'}x_{i'} + n \end{aligned} \tag{7}$$

where $\boldsymbol{g}_{ki'}$ is the Rayleigh channel vector between the i'-th interfering MBSA and the k-th UE.

2) Indoor Links: Due to the random position of the indoor UE, the IAP can only select beam vectors with the closest AoD for each UE to match its position in the angular domain, i.e., $|\theta_{m_q} - \theta_q| \leq 1/M_T'$. The transmitted signal of an IAP is given by

$$\boldsymbol{x} = \sum_{q=1}^{N_{\text{iue}}}\boldsymbol{b}_q s_q \tag{8}$$

where $\boldsymbol{b}_q = \boldsymbol{a}^*(\theta_{m_q})$ is the beam vector for the q-th indoor UE. Since the indoor scenario is completely separate from the outdoor scenario, we omit the indices indicating the area and the building to aid clarity. Due to the high path-loss of mmWave signals, the indoor user only suffers from interference of other indoor users within the same building. The received signal at the q-th UE can be given by

$$\begin{aligned} r_q &= \mathbf{a}^T_{M_{R_q}}(\phi_q)\mathbf{g}_q\mathbf{b}_{m_q}s_q + \sum_{j=1 j\neq q}^{N_{\text{iue}}}\mathbf{a}^T_{M_{R_q}}(\phi_q)\mathbf{g}_q\mathbf{b}_{m_j}s_j + n \\ &= \sqrt{\beta_q M_{Rq} M_{Tq}}\mathbf{a}^T_{M_{T_q}}(\theta_q)\mathbf{a}^*_{M_{T_q}}(\theta_{m_q})s_q \\ &\quad + \sqrt{\beta_q M_{Rq} M_{Tq}}\sum_{j=1 j\neq q}^{N_{\text{iue}}}\mathbf{a}^T_{M_{T_q}}(\theta_q)\mathbf{a}^*_{M_{T_j}}(\theta_{m_j})s_j + n. \end{aligned} \tag{9}$$

III. Spectrum-Energy-Economy Efficiency Analysis

A. Spectrum Efficiency

The SE can be defined as the ratio of the system capacity over the link bandwidth, with the expression as

$$\eta_{SE} = \frac{C}{B} \tag{10}$$

where B is the bandwidth and C is the capacity of the system. As defined by the Shannon equation, the system capacity can be expressed as

$$C = \mathbb{E}\left[B\log_2(1 + \text{SINR})\right]. \tag{11}$$

For massive MIMO systems, following the approximation derived in [39], we can assume that $\mathbb{E}\left[B\log_2(1 + \text{SINR})\right] \approx B\log_2(1 + \mathbb{E}[\text{SINR}])$. So, the SE analysis can be deduced from the analyses of $\mathbb{E}[\text{SINR}]$, i.e., the expectation of signal

$$\mathbb{E}\left[{\text{SINR}_{\ell ji}}^{M\to B}\right] \approx \frac{\mathbb{E}\left[\left(\sqrt{\beta_{\ell ji}M_T M_R}s_{\ell ji}\right)^2\right]}{\mathbb{E}\left[\left(\sqrt{\beta_{\ell ji}M_T M_R}\sum_{k=1}^{N_{\text{oue}}}\boldsymbol{a}^T_{M_T}(\theta_{\ell ji})\boldsymbol{w}_{ki}s_{ki}\right)^2\right] + \mathbb{E}\left[\left(\sum_{i'\in N(i)}\boldsymbol{a}^{\mathrm{T}}_{M_R}(\phi_{\ell ji})\boldsymbol{G}_{\ell' j' i'}\boldsymbol{x}_{i'}\right)^2\right] + \mathbb{E}[|n|^2]}. \tag{12}$$

to interference plus noise power ratio (SINR). $\mathbb{E}$[SINR] of the three types of constituent links are analyzed in the following.

The expectation of receiving SINR over the l-th link between the i-th MBSA and j-th BMAA can be expressed as in (12), shown at the bottom of the previous page.

According to the received signal over the l-th beamforming channels at the j-th BMAA, since the mean of $s_{\ell ji}$, s_{ki} and s_q is zero, the total average normalized power is equal to the variance $P_{\ell ji}$, P_{ki} and P_q, i.e., $\mathbb{E}[s_{\ell ji}^2] = P_{\ell ji}$, $\mathbb{E}[s_{ki}^2] = P_{ki}$, and $\mathbb{E}[s_q^2] = P_q$.

Based on the assumptions,

$$\mathbb{E}\left[\left[\sqrt{\beta_{\ell ji} M_R M_T} s_{\ell ji}\right]^2\right] = \beta_{\ell ji} M_R M_T P_{\ell ji} \tag{13}$$

$$\begin{aligned}\mathbb{E}&\left[\left[\sqrt{\beta_{\ell ji} M_R M_T}\sum_{k=1}^{N_{oue}} \mathbf{a}_{MT}^T(\theta_{\ell ji})\omega_{ki}s_{ki}\right]^2\right]\\ &= \frac{\beta_{\ell ji}M_R}{M_T}\mathbb{E}\left[\left[\sum_{m=1}^{M_T}\sum_{k=1}^{N_{oue}} h_{ki}^* s_{ki} e^{-j2\pi\Delta(m-1)sin\theta_{\ell ji}}\right]^2\right]\end{aligned} \tag{14}$$

$$\begin{aligned}\mathbb{E}&\left[\left[\sum_{i'\in\mathcal{N}[i]}\mathbf{a}_{MR}^T[\phi_{\ell ji}]\,\mathbf{G}_{\ell' j' i'} x_{i'}\right]^2\right]\\ &= \frac{\beta_{\ell' j' i'} M_T'}{M_R}\mathbb{E}\\ &\times\left[\left(\sum_{i'\in\mathcal{N}(i)}\left(\frac{1-e^{-j2\pi\Delta M_R[\sin\phi_{\ell ji}-\sin\phi_{\ell' j' i}]}}{1-e^{-j2\pi\Delta[\sin\phi_{\ell ji}-\sin\phi_{\ell' j' i}]}} s_{\ell' j' i}\right.\right.\right.\\ &+\frac{1-e^{-j2\pi\Delta M_R[\sin\phi_{\ell ji}-\sin\phi_{\ell' j' i}]}}{1-e^{-j2\pi\Delta[\sin\phi_{\ell ji}-\sin\phi_{\ell' j' i}]}}\\ &\left.\left.\left.\times\frac{1}{M_T'}\sum_{m=1}^{M_T'}\sum_{k=1}^{N_{oue}} h_{ki'}^* s_{ki'} e^{-j2\pi\Delta(m-1)sin\theta_{\ell' j' i'}}\right)\right)^2\right].\end{aligned} \tag{15}$$

The derivations of (14) and (15) are detailed in the appendix. For all the noise power, $\mathbb{E}\left[|n|^2\right] = \sigma_n^2$. Hence, the expectation of the receiving SINR over the l-th link between the i-th MBSA and j-th BMAA can be obtained.

Following a similar method for the indoor connection, the expectation of receiving SINR over the u-th link between the IAP and q-th indoor users can be expressed in (16), shown at the bottom of the page.

We find that only other indoor users within the same building can generate interference to an indoor user. To simplify the system model, we assume a uniform antenna configuration for all IAPs. As a result, we have $M_{Tq} = M_{Tj}$.

$$\begin{aligned}\mathbb{E}&\left[\left[\sqrt{\beta_q M_{Rq} M_{Tq}}\mathbf{a}_{M_{Tq}}^T[\theta_q]\,\mathbf{a}_{M_{Tq}}^*[\theta_{m_q}]\,s_q\right]^2\right]\\ &= \frac{\beta_q M_{Rq} P_q}{M_{Tq}}\left(\frac{1-e^{-j2\pi\Delta M_{Tq}[\sin\theta_q-\sin\theta_{m_q}]}}{1-e^{-j2\pi\Delta[\sin\theta_q-\sin\theta_{m_q}]}}\right)^2\end{aligned} \tag{17}$$

$$\begin{aligned}\mathbb{E}&\left[\left[\sqrt{\beta_q M_{Rq} M_{Tq}}\sum_{j=1 j\neq q}^{N_{\text{iue}}}\mathbf{a}_{M_{Tq}}^T[\theta_q]\,\mathbf{a}_{M_{Tj}}^*[\theta_{m_j}]\,s_j\right]^2\right]\\ &= \frac{\beta_q M_{Rq} P_j}{M_{Tq}}\mathbb{E}\left[\left[\sum_{j=1 j\neq q}^{N_{\text{iue}}}\frac{1-e^{-j2\pi\Delta M_{Tq}[\sin\theta_q-\sin\theta_{m_j}]}}{1-e^{-j2\pi\Delta[\sin\theta_q-\sin\theta_{m_j}]}}\right]^2\right].\end{aligned} \tag{18}$$

For links between MBSA and outdoor UE, the normalized precoding vector is $\boldsymbol{w}_{ki} = \boldsymbol{h}_{ki}^*/\sqrt{M_T}$. By applying it to (7), the expectation of received SINR of the k-th outdoor UE is in (19), shown at the bottom of the page.

B. Energy Efficiency

The EE η_{EE} of one cell is defined as the capacity divided by the total system power consumption, i.e.,

$$\eta_{EE} = \frac{C}{P_{\text{cell}}} \tag{20}$$

which indicates the efficiency of converting the power into data traffic. The power consumption should include all devices deployed inside the cell. In the case of separating indoor and outdoor scenarios, the power consumed by MBS, MBSA,

$$\mathbb{E}\left[\mathbf{SINR}_{uq}^{IAP\to I}\right] \approx \frac{\mathbb{E}\left[\left[\sqrt{\beta_q M_{Rq} M_{Tq}}\mathbf{a}_{M_{Tq}}^T[\theta_q]\,\mathbf{a}_{M_{Tq}}^*[\theta_{m_q}]\,s_q\right]^2\right]}{\mathbb{E}\left[\left[\sqrt{\beta_q M_{Rq} M_{Tq}}\sum_{j=1 j\neq q}^{N_{\text{iue}}}\mathbf{a}_{M_{Tq}}^T[\theta_q]\,\mathbf{a}_{M_{Tj}}^*[\theta_{m_j}]\,s_j\right]^2\right]+\mathbb{E}\left[|n|^2\right]}. \tag{16}$$

$$\begin{aligned}\mathbb{E}[\text{SINR}_{ki}^{M\to U,P}] \approx &\frac{\beta_{ki}\mathbb{E}[|\boldsymbol{h}_{ki}^T\boldsymbol{h}_{ki}^*|^2]P_{ki}}{\beta_{ki}\left(\sum_{j=1,j\neq k}^{N_{\text{oue}}}\mathbb{E}[|\boldsymbol{h}_{ki}^T\boldsymbol{h}_{ji}^*|^2]P_{ki}+\sum_{j=1}^{N_a}\sum_{\ell=1}^{L}\mathbb{E}[|\boldsymbol{h}_{ki}^T\boldsymbol{a}^*(\theta_{\ell ji})|^2]\right)}\\ &+\frac{}{\beta_{ki'}\sum_{i'\in\mathcal{N}(i)}\left(\sum_{k'=1}^{N_{\text{oue}}}\mathbb{E}[|\boldsymbol{h}_{ki}^T\boldsymbol{h}_{k'i'}^*|^2]P_{k'i'}+\sum_{j=1}^{N_a}\sum_{\ell=1}^{L}\mathbb{E}[|\boldsymbol{h}_{ki}^T\boldsymbol{a}(\theta_{\ell' j' i'})|^2P_{\ell' j' i'}\right)+\mathbb{E}[|n|^2]}.\end{aligned} \tag{19}$$

BMAA, and IAP should be taken into account as follows

$$P_{\text{cell}} = P_{\text{tot}}^{\text{MBS}} + \sum_{i=1}^{N_a} (P_{\text{tot}}^{\text{BMAA}} + P_{\text{tot}}^{\text{IAP}}). \tag{21}$$

A high-level EE evaluation framework (E^{3}F) for mobile communication systems has been investigated and developed in [40]. Based on this framework, the general energy consumption model of a base station is given by

$$P_{\text{sys}} = P_{\text{BB}} + P_{\text{RF}} + P_{\text{PA}} + P_{\text{OH}} \tag{22}$$

where P_{BB} represents the power consumed by digital baseband processing, P_{RF} and P_{PA} are power consumed by the RF front-end and the power amplifier (PA), and P_{OH} represents other system power overhead consumed by the system including the cooling and alternating current (AC)-direct current (DC) converters.

The digital baseband processing section also includes the digital signal processing, system control, and networking related processes. For the digital signal processing, its operations include the digital filtering, up/down sampling, (Inverse) Fast Fourier transform ((I)FFT), MIMO channel estimation, orthogonal frequency-division multiplexing (OFDM) modulation/demodulation, symbol mapping, and channel encoding/decoding. The operation complexity, denoted by $\mathcal{O}$, is measured by Giga floating-point operations per second (GFO/s), depending on the type of the operation, the number of UE, and the data streams. The power consumption per Giga floating-point operation is further scaled by a technology-dependent factor ρ. Thus, P_{BB} can be obtained through dividing GFO/s by ρ.

The key constituent components of the RF part include carrier modulators, frequency synthesis, clock generators, digital to analogue (DA) /analogue to digital (AD) converters, mixer, and so on. The power consumption of these components scales with parameters system bandwidth, number of antennas, and the traffic load.

The power consumption model of a PA depends on the PA type, the maximum output power, and the actual output power that assures the desired SE. In this work, we consider two types of PAs. One is the class-B PA which is deployed on the MBSA and BMAA and enables transmissions at a relatively high output power. The other one is the Doherty PA developed for high-frequency band communication systems that require high power efficiency. This type of PA is employed by the IAP here.

Explicit power models for MBS, BMAA, and IAP are introduced as follows.

1) Power Consumption Model of MBS: The total consumed power of MBS is given by

$$P_{\text{tot}}^{\text{MBS}} = \frac{P_{\text{BB}}^{\text{MBS}} + N_a P_{\text{tot}}^{\text{MBSA}}}{(1-\eta_{\text{c}})(1-\eta_{\text{ac-dc}})(1-\eta_{\text{dc-dc}})} \tag{23}$$

where $P_{\text{BB}}^{\text{MBS}}$ is the power of the digital baseband process at the MBS, $P_{\text{tot}}^{\text{MBSA}}$ is the power consumed by each MBSA, η_{c}, $\eta_{\text{ac-dc}}$, and $\eta_{\text{dc-dc}}$ are power efficiency of the cooling system, AC-DC and DC-DC conversions, respectively.

Based on the outdoor distributed antenna architecture, the digital baseband signal processing at the MBS includes mapping/de-mapping of symbols, channel encoding ($\mathcal{O}_{\text{enc}}$), upper layer network ($\mathcal{O}_{\text{nw}}$), and control operations ($\mathcal{O}_{\text{ctrl}}$) for the N_a MBSA, respectively. Thus, $P_{\text{BB}}^{\text{MBS}}$ can be further written by

$$P_{\text{BB}}^{\text{MBS}} = \sum_{i=1}^{N_a} (\mathcal{O}_{\text{ctrl},i} + \mathcal{O}_{\text{nw},i} + \mathcal{O}_{\text{enc},i})/\rho. \tag{24}$$

2) Power Consumption Model of MBSA: The power consumption of MBSA can be decomposed as

$$P_{\text{tot}}^{\text{MBSA}} = P_{\text{BB}}^{\text{MBSA}} + P_{\text{RF}}^{\text{MBSA}} + P_{\text{PA}}^{\text{MBSA}}. \tag{25}$$

For each MBSA, the downlink baseband signal processing includes filtering, up sampling, (I)FFT of OFDM symbols, massive MIMO channel estimation, precoding/beamforming, symbol mapping, and control plus other network relation operations. It can be written as

$$\begin{aligned} P_{\text{BB}}^{\text{MBSA}} = (&\mathcal{O}_{\text{fltr}} + \mathcal{O}_{\text{smpl}} + \mathcal{O}_{\text{fft}} + \mathcal{O}_{\text{est}} + \mathcal{O}_{\text{bf}} + \mathcal{O}_{\text{pre}} \\ &+ \mathcal{O}_{\text{map}} + \mathcal{O}_{\text{ctrl}} + \mathcal{O}_{\text{nw}})/\rho. \end{aligned} \tag{26}$$

In (26), the complexity of (I)FFT can be scaled by $\mathcal{O}_{(\text{i})\text{fft},i} = N_{\text{s}} N_{(\text{i})\text{fft}} \log_2(N_{(\text{i})\text{fft}})$, where $N_{(\text{i})\text{fft}}$ is the number of sub-carriers of one OFDM symbol, and N_{s} is the total number of OFDM symbols. The complexity of channel estimation by using the correlation of orthogonal pilot sequences can be scaled by $\mathcal{O}_{\text{est}} = M_T N_{\text{ue}}^2$ with N_{ue} presents the number of UEs. The complexity of the channel precoding and beamforming operation can be scaled by $\mathcal{O}_{\text{bf/pre}} = (N_{\text{oue}} + N_b L)(1 - N_{\text{ue}}/N_{\text{c}})$ for the uplink channel estimation. Note that N_{c} represents the number of channel resource blocks related to the coherence time and coherence bandwidth. For the operation complexity of the remaining processes, some typical values are adopted.

For the RF part of the MBSA, its analog components include the modulator, mixer, clock generator, and the digital to analog converter. The power consumption of this part is given by

$$\begin{aligned} &P_{\text{RF}}^{\text{MBSA}} \\ &\quad = M_T (P_{\text{mod}}^{\text{MBSA}} + P_{\text{mix}}^{\text{MBSA}} + P_{\text{dac}}^{\text{MBSA}}) + \sqrt{M_T} P_{\text{clk}}^{\text{MBSA}}. \end{aligned} \tag{27}$$

Please note that the power consumptions of the modulator, mixer, and DAC can be linearly scaled with the number of antennas [41], [42]. The clock generator can be scaled by the square root of the number of antennas [43], [44].

For the PA, its power consumption can be calculated as

$$P_{\text{PA}}^{\text{MBSA}} = \frac{1}{\eta_B} \tag{28}$$

where η_B is defined by

$$\eta_B = \frac{\pi}{4} \frac{r_o^2}{r_{\max} \mathbb{E}[r_o]} \tag{29}$$

as the power efficiency of the class-B PA. In (29), r_{o} and $r_{\max}$ represent the amplitude and the maximum amplitude of the output signal, respectively. We have $r_{\text{o}} = \sqrt{P_{\text{o}}}$, and $r_{\max} = \sqrt{P_{\max}}$ with P_{o} and $P_{\max}$ being the output power and maximum output power, respectively.

3) Power Consumption Model of BMAA: The power consumption model of BMAA can be written as

$$P^{\mathrm{BMAA}} = \frac{P_{\mathrm{BB},\ell}^{\mathrm{BMAA}} + M_R P_{\mathrm{RF}}^{\mathrm{BMAA}}}{(1-\eta_{\mathrm{c}})(1-\eta_{\mathrm{ac-dc}})(1-\eta_{\mathrm{dc-dc}})}. \tag{30}$$

In the downlink, each BMAA receives the traffic from the serving MBSA over L beamformed data links and forwards it to IAP. Therefore, the baseband data process consists of filtering, receive beamforming process, down sampling, IFFT process, symbol demapping, channel decoding, control and network processes. Its GOP/S can be estimated similarly as the case of MBSA, i.e.,

$$P_{\mathrm{BB}}^{\mathrm{BMAA}} = L \cdot (\mathcal{O}_{\mathrm{fltr}} + \mathcal{O}_{\mathrm{bf}} + \mathcal{O}_{\mathrm{smpl}} + \mathcal{O}_{\mathrm{ifft}} + \mathcal{O}_{\mathrm{demap}} + \mathcal{O}_{\mathrm{dec}} + \mathcal{O}_{\mathrm{ctrl}} + \mathcal{O}_{\mathrm{nw}})/\rho. \tag{31}$$

The analogue components of the downlink RF front end include mixer, clock, variable gain amplifiers (VGA), ADC, and the low-noise amplifier (LNA). Therefore, we have

$$P_{\mathrm{RF}}^{\mathrm{BMAA}} = M_R \cdot (\mathcal{O}_{\mathrm{mix}} + \mathcal{O}_{\mathrm{vga}} + \mathcal{O}_{\mathrm{adc}} + \mathcal{O}_{\mathrm{lna}}) + \sqrt{M_R}\mathcal{O}_{\mathrm{clc}}. \tag{32}$$

Please note that the power consumption LNA and VGA over the receiving RF FE are considered as constant, which is unlike the PA used for signal transmission.

4) Power Consumption Model of IAP: The IAP is similar to pico or femto base stations, which are much smaller and simpler compared with conventional base station. It usually employs a low-power architecture. The power consumption of the IAP is given as

$$P_{\mathrm{tot}}^{\mathrm{IAP}} = \frac{P_{\mathrm{BB}}^{\mathrm{IAP}} + M_T'(P_{\mathrm{RF}}^{\mathrm{IAP}} + P_{\mathrm{PA}}^{\mathrm{IAP}})}{(1-\eta_{\mathrm{c}})(1-\eta_{\mathrm{ac-dc}})(1-\eta_{\mathrm{dc-dc}})}. \tag{33}$$

For the downlink of the IAP, we consider a constant power consumption for baseband process, as the number of UE for a IAP is much fewer than the MBSA, so the baseband process is not as sophisticated as that of the outdoor base stations. The RF chain includes the mixer, DAC, filter, phase shifter (PS), and the clock. Its consumed power can be expressed as

$$P_{\mathrm{RF}}^{\mathrm{IAP}} = M_T'(P_{\mathrm{mix}}^{\mathrm{IAP}} + P_{\mathrm{dac}}^{\mathrm{IAP}} + P_{\mathrm{bft}}^{\mathrm{IAP}} + P_{\mathrm{fs}}^{\mathrm{IAP}}) + \sqrt{M_T'}P_{\mathrm{clc}}^{\mathrm{IAP}}. \tag{34}$$

The power consumption of the Doherty PA can be computed directly by

$$P_{\mathrm{PA}}^{\mathrm{IAP}} = \begin{cases} \frac{2}{\pi}\sqrt{P_{\mathrm{o}}P_{\max}^{\mathrm{IAP}}}, & 0 < P_o < 0.25P_{\max}^{\mathrm{IAP}} \\ \frac{6}{\pi}\sqrt{P_{\mathrm{o}}P_{\max}^{\mathrm{IAP}}}, & 0.25P_{\max}^{\mathrm{IAP}} \le P_o \le P_{\max}^{\mathrm{IAP}}. \end{cases} \tag{35}$$

C. Economic Efficiency

The ECE of a cell is defined as the net revenue per second, i.e., the earnings from effective data throughput minus the operational cost. In this paper, we adopt the practical ECE model proposed by [31], i.e.,

$$\varepsilon_{\mathrm{cell}} = \sum_{v=1}^{V} \kappa_v U(v, R_v) - (C_0 + \kappa_c P_{\mathrm{cell}}). \tag{36}$$

On the right-hand side of (36), the first part represents the earnings, which is dependant on the type of traffic v, the effective data throughput $U(v, R_v)$, and the revenue per bit of traffic κ_v. The second part is the expenditure of network operation, including the fixed cost of maintenance per second C_0 and the expenses on electricity computed by multiplying the energy cost per Joule and the power consumed by the equipment, represented by κ_c and P_{cell}, respectively.

ECE can be considered here as a complement to SE and EE. We observe that ECE integrates the SE and EE, as the earnings are associated with the SE and the cost is mainly related to the power consumption. Therefore, ECE potentially offers a method to find the right trade-off between SE and EE. For the earnings part, the traffic is categorized into several different classes each of which is charged on a different basis, ensuring the model is representative of the real network. In this paper, the traffic is categorized into $v = 3$ classes. Class-1 represents the data traffic generated by voice services, which is charged linearly. In addition, this class has an upper limit imposed. This is for two reasons: 1) it has been reported that voice service is approaching saturation level; 2) the network cannot dedicate all its resource to serve the traffic of the most stringent QoS. Therefore, once this limit is exceeded call loss is permitted. Class-2 traffic are the bundled data services with limited quota, whose attainable revenue grow in a logarithmic fashion proportional to the data volume. A logarithmic basis is adopted to scale the traffic based on the observation that the price per bit of higher quota bundles should be less than that of the lower quota service bundles. Class-3 is the traffic of the service bundle where the user is entitled to an unlimited quota of data traffic. The contribution of each traffic class to the total throughput of the cell R_{cell} is given by

$$R_v = \begin{cases} \min\left\{R_1^{\mathrm{lim}}, \alpha_1 R_{\mathrm{cell}}\right\}, & v = 1 \\ \alpha_2 R_{\mathrm{cell}}, & v = 2 \\ R_{\mathrm{cell}} - R_1 - R_2, & v = 3 \end{cases} \tag{37}$$

where α_1 and α_2 are the percentages of the Class-1 and Class-2 traffic, respectively, and R_1^{lim} is the upper limit for traffic Class-1. These characteristics of the traffic are further defined by the utility function $U(v, R_v)$ as

$$U(v, R_v) = \begin{cases} R_1, & v = 1 \\ R_2^{\mathrm{ref}} \log_2(1 + \frac{R_2}{R_2^{\mathrm{ref}}}), & v = 2 \\ R_3^{\mathrm{ref}} u(R_3), & v = 3 \end{cases} \tag{38}$$

where R_2^{ref} and R_3^{ref} are the referenced data rates for traffic Class-2 and Class-3, respectively, and $u(.)$ is the Heaviside step function. The values of these parameters are summarized in Table I. Note that (38) maps the real traffic volume onto chargeable traffic and enables the revenue to be computed.

TABLE I
ECE Related Parameters

Parameter	Value	Parameter	Value
R_1^{lim}	400 Mbps	κ_1	1.43×10^{-5} pence/bit
R_2^{ref}	240 Mbps	κ_2	7.76×10^{-6} pence/bit
R_3^{ref}	4 Gbps	κ_3	2.93×10^{-7} pence/bit
α_1	1%	κ_c	4.22×10^{-6} pence/J
α_2	80%	C_0	4.15×10^{-7} pence/s

TABLE II
System Simulation Parameters

Parameter	Value	Parameter	Value
M_T	256	M_R	32
M_T'	16	L	6
N_b	3	$\mathcal{N}(i)$	6
N_{oue}	4	N_{iue}	12
V_{oue}	10.8 km/h	N_{c}	196
B_c	210 kHz	N_{s}	1.4×10^4
f_c	2.6 GHz	f_{cmm}	28 GHz

IV. Results and Discussions

A. Simulation Parameters

For the outdoor coverage, a standard 20 MHz LTE system is considered as the reference system, the carrier frequency of which is configured as 2.6 GHz. All the key parameters are listed in Table II.

The highest mobility speed that the LTE system can support is 350 km/h, which is the speed of a high-speed train. In the urban areas, a UE generally does not move very fast, so the highest speed is set to be 10.8 km/h. With the carrier frequency of 2.6 GHz, the coherence time of the assumed channel is around 2.3 ms, which is equivalent to the duration of 14 OFDM symbols. The length of the cyclic prefix (CP) of an OFDM symbol is defined to be 5.2 μs, which is the maximal delay spread the system can tolerate. The coherent bandwidth can be computed to be around 210 kHz, which is equivalent to the bandwidth of 14 consecutive sub-carriers. Therefore, the wireless channel in the assumed urban environment can be considered to be static for every $14 \times 14 = 196$ channel resource blocks, i.e., $N_{\text{c}} = 196$.

In a macro cell, each MBSA serves 4 outdoor UE plus 3 buildings, and suffers from interference from 6 neighboring MBSAs, i.e., $\mathcal{N}(i) = 6$. Each BMAA is equipped with 32 antennas. For each of the MBSA and BMAA pair, there are 6 beamforming links. For each BMAA, as expressed in (6), it suffers from the interference from the signal intended to be received by the 4 outdoor UEs in the same cell, and the interference from the 6 neighboring MBSAs, which are simulated as (5). Inside each building, there are 12 indoor UE that require network access, so the interference signals are simulated as (8). Each IAP is equipped with an antenna array of 16 elements, and operates in the 28 GHz band with a signal bandwidth of 500 MHz. Here, the IAP is assumed to operate in a similar fashion to an 802.11ad-like system, where each indoor UE is served simultaneously in the downlink over a dedicated beam allocated by IAP.

For both scenarios, it is assumed that all UE require the same downlink data rate, so that a homogeneous QoS is assumed across the cell.

1) Path Loss Model and Noise Power: The path loss model of four types of links are summarized in Table III. For the link between MBSAs and BMAAs, the WINNER II B5a model [45] is adopted. For the link between MBSA and outdoor UE, WINNER-II C2 urban macro-cell NLOS model is adopted. For indoor links, we adopt the model proposed in [46], where the path loss exponent is set to 2 which is the average value for indoor mmWave propagation environment. For the link between the MBSA and indoor UE in the non-separate scenarios, the same model of the link between outdoor UE is adopted except that a 20 dB penetration loss is added to the loss. Equal average distances are assumed for links from the MBSA to the BMAA and outdoor UE in scenario A, the links between IAP and indoor UE for scenario B.

The noise power is computed by the

$$\sigma_n^2 = kTB + D \tag{39}$$

which is the model adopted for LTE link budget estimation in [47]. In (39), k represents the Boltzmann constant, T is temperature of the surrounding environment in Kelvin, which is set to be 290 K, i.e. 17 °C, B is the system bandwidth in Hz, D is the noise figure. The value of D depends on the types of receiving equipment, which is 2 dB for the MBSA, BMAA, and IAP, 7 dB for indoor and outdoor UE.

2) Operation Complexity and Power Consumption Parameters: The referenced process complexity and power consumption of the components are listed in Table IV and V, respectively. We refer to [43] for the operation complexity of processes including filtering, sampling, symbol mapping and de-mapping, encoding and decoding, network and control.

The power consumption parameters of the analog components of MBSA and BMAA are based on the typical valued proposed in [44] for LTE base stations and the modification for massive MIMO system [43]. For a mmWave IAP, the typical parameters proposed in [48] are adopted in this paper. Besides, the transmitted power of the UE for sending the uplink pilot symbols is assumed as 20 dBm in this work.

B. Capacity Analysis

The comparison between the conventional, non-separated (referred to as the one-link), network architecture and the separated ones (referred to as the two-link) in terms of the capacity is shown in Fig. 2(a). The comparison clearly indicates excellent agreement between the theoretical derivation and simulation results, providing confidence in the theoretical derivation. As the capacity is the basis for further investigations such as the EE and SE analysis, this provides confidence in the rest results. If we further compare the one-link solution with the two-link results, it is clear that the indoor-outdoor separated solution can provide a higher achievable capacity than the conventional direct transmission as there is no penetration loss. The improvement in system performance is more obvious when the indoor communication adopts mmWave and beamforming technology, which reduces the interference. As we considered the interference in this work, the capacity will hit a limit when the SNR value is high due to the interference dominating the system performance.

The speed that the system approaches this limit is an important benchmark to the evaluation. Here, we use the

TABLE III
PATH LOSS MODEL

Link type	**Path loss model**	f_c	d
MBSA-BMAA	$23.5\log_{10}(d) + 42.5 + 20\log_{10}(f_c/5.0)$	2.6 GHz	500 m
MBSA-Outdoor UE	$(44.9 - 6.55\log_{10}(h_{bs}))\lg(d) + 34.46 + 5.83\log_{10}(h_{bs}) + 23\log_{10}(f_c/5.0)$	2.6 GHz	500 m
MBSA-Indoor UE	$PL_{\mathrm{MBSA-OutdoorUE}} - 20$	-	-
IAP-Indoor UE	$20\log_{10}(4\pi/c) + 20\log_{10}(d)$	28 GHz	15 m

TABLE IV
REFERENCED COMPLEXITY OF BASEBAND OPERATIONS

Parameter	**GOP/s**	**Parameter**	**GOP/s**
$\mathcal{O}_{\mathrm{(i)fft}}$	$N_{\mathrm{s}}N_{\mathrm{(i)fft}}\log_2(N_{\mathrm{(i)fft}}) \times 10^{-9}$	$\mathcal{O}_{\mathrm{smpl}}$	$2.0 \cdot M_T$
$\mathcal{O}_{\mathrm{est}}$	$M_T N_{\mathrm{ue}}\tau\frac{N_{\mathrm{re}}}{N_{\mathrm{c}}} \times 10^{-9}$	$\mathcal{O}_{\mathrm{(de)map}}$	$1.3 \cdot (N_{\mathrm{ue}} + N_b L)N_{\mathrm{re}}$
$\mathcal{O}_{\mathrm{bf}}$	$M_T N_b L N_{\mathrm{re}}(1 - \frac{\tau}{N_{\mathrm{c}}}) \times 10^{-9}$	$\mathcal{O}_{\mathrm{fltr}}$	$6.7 \cdot M_T$
$\mathcal{O}_{\mathrm{pre}}$	$M_T N_{\mathrm{ue}} N_{\mathrm{re}}(1 - \frac{\tau}{N_{\mathrm{c}}}) \times 10^{-9}$	$\mathcal{O}_{\mathrm{det}}$	$N_{\mathrm{ue}}N_{\mathrm{re}} \times 10^{-9}$
$\mathcal{O}_{\mathrm{ctrl}}$	$2.7(N_{\mathrm{ue}} + N_b L)N_a$	$\mathcal{O}_{\mathrm{nw}}$	$8.0 \cdot (N_{\mathrm{ue}} + N_b L)N_a$
$\mathcal{O}_{\mathrm{enc/dec}}$	$1.3(N_{\mathrm{ue}} + N_b L)N_a$	ρ	160 GOP/W

TABLE V
REFERENCE POWER CONSUMPTION OF ANALOG COMPONENTS

MBSA		**BMAA**		**IAP**	
Parameter	**Value**	**Parameter**	**Value**	Parameter	**Value**
$P_{\mathrm{mod}}^{\mathrm{MBSA}}$	125 mW	$P_{\mathrm{vga}}^{\mathrm{BMAA}}$	63 mW	$P_{\mathrm{fs}}^{\mathrm{IAP}}$	20 mW
$P_{\mathrm{mix}}^{\mathrm{MBSA}}$	200 mW	$P_{\mathrm{mix}}^{\mathrm{BMAA}}$	200 mW	$P_{\mathrm{mix}}^{\mathrm{IAP}}$	23 mW
$P_{\mathrm{dac}}^{\mathrm{MBSA}}$	225 mW	$P_{\mathrm{adc}}^{\mathrm{BMAA}}$	100 mW	$P_{\mathrm{dac}}^{\mathrm{IAP}}$	75 mW
$P_{\mathrm{clk}}^{\mathrm{MBSA}}$	75 mW	$P_{\mathrm{clk}}^{\mathrm{BMAA}}$	75 mW	$P_{\mathrm{clc}}^{\mathrm{IAP}}$	5 W
$P_{\mathrm{max}}^{\mathrm{MBSA}}$	1 W	$P_{\mathrm{lna}}^{\mathrm{BMAA}}$	125 mW	$P_{\mathrm{max}}^{\mathrm{IAP}}$	50 mW
System overhead factors					
η_{c}	10%	$\eta_{\mathrm{ac-dc}}$	5%	$\eta_{\mathrm{dc-dc}}$	10%

cumulative distribution function (CDF) of the capacity to study this criterion. The CDF of the capacity for the three cases is shown in Fig. 2(b). From the CDF, we can observe that the two-link with mmWave solution has a much larger upper bound compared with the other two systems, which indicates this system may provide a much better performance in terms of the system throughput.

From this comparison, we can conclude that for the 5G and B5G wireless networks, both the network architecture and the access technologies should both be considered in order to achieve a global optimization of different system performance metrics. The interference management is always the key issue to ensure improved system performance.

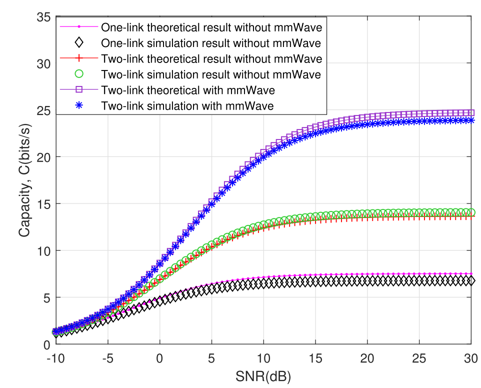

(a) Comparison of capacities

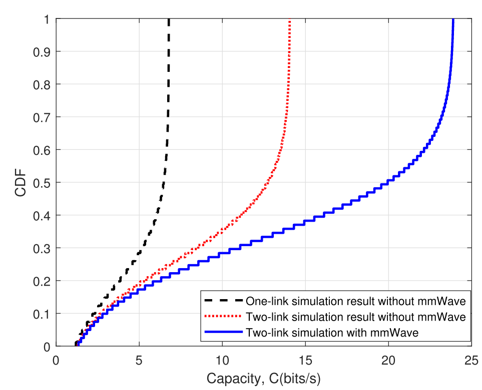

(b) Comparison for CDF of capacities

Fig. 2. Comparison of capacities for one-link and two-link network architectures with and without mmWave technology.

C. SE, EE, and ECE Results Analysis

From the simulation results shown in Fig. 3(a), we conclude that the separate indoor and outdoor scenario can provide a higher SE than direct transmission with the same SNR. When mmWave technology is utilized, the SE can be further improved due to lower interference. When the SNR is 30 dB, the SE of the two-link architecture with mmWave can achieve 1.72 bits/s/Hz, while the SE of the traditional network architecture is 0.49 bits/s/Hz. This gain will be more evident as the SNR increases.. Similar conclusions can be drawn from the SE CDF comparison in Fig. 3(b). We note that the two-link with mmWave solution has a much larger increasing room in terms of the SE compared with other

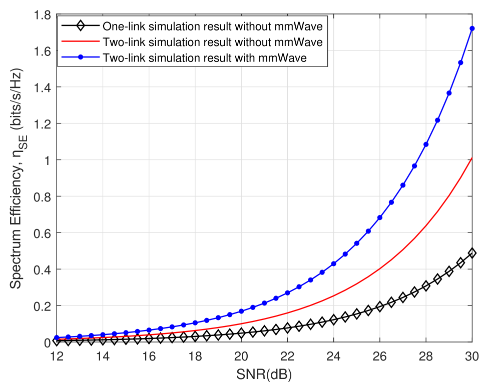

(a) Comparison of SE

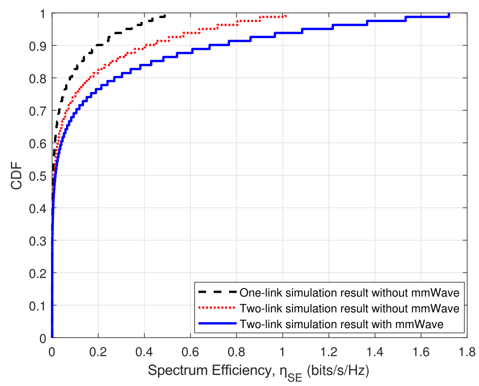

(b) Comparison for CDF of SE

Fig. 3. Comparison of SE for one-link and two-link network architectures with and without mmWave technology.

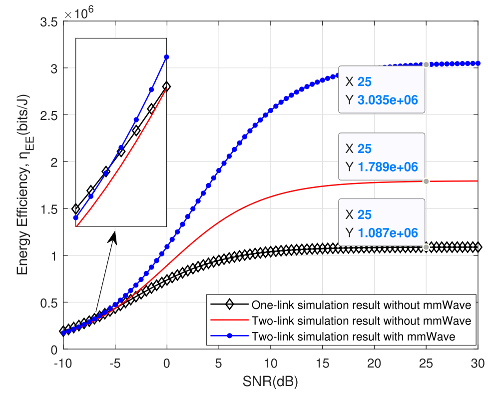

(a) Comparison of EE

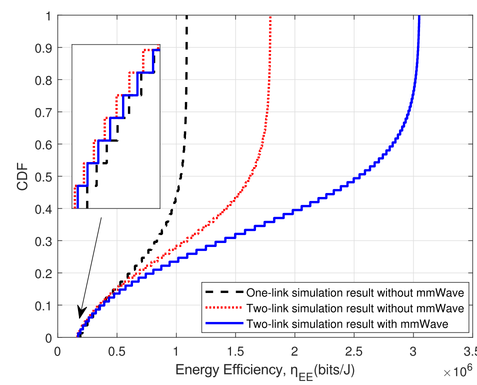

(b) Comparison for CDF of EE

Fig. 4. Comparison of EE for one-link and two-link network architectures with and without mmWave technology.

solutions. For a two-link with mmWave solution, its advantage in penetration loss elimination and interference management is the main reason for its superior performance.

The EE of these three cases is compared in Fig. 4(a). In general, the two-link solution especially with the mmWave technology is advantageous in terms of EE as indoor users only need to communicate with the indoor IAPs. It can avoid the penetration loss and provide a much better interference management. The EE curves converge when the SNR exceeds 25 dB, and the proposed network architecture provides three times gain of the EE compared to the one-link architecture. It is interesting to note that in the case of very low SNR range, the one-link solution offers a better performance. This is because for the EE, its consumed power includes both the standby power and the transmit power. For the two-link solution, due to more components, its standby power consumption is much higher. Nevertheless, the increased speed of system capacity for the two-link solution is much faster than the one-link system, which can overcome the higher consumption. We also observe from the comparison for the EE CDF in Fig. 4(b), that it is clear that the EE of the one-link system reaches its limit much quicker than the two-link system, and the utilisation of mmWave technology can further enhance and improvement of the system performance in terms of EE due to avoiding the penetration loss and better interference management.

Fig. 5(a) and Fig. 5(b) illustrate the SE and EE of the three architectures with 12 outdoor UEs and 4 indoor UEs. Fig. 3(a) and Fig. 4(a) demonstrate the SE and EE with 4 outdoor UEs and 12 indoor UEs. Since the total number of UEs is the same, Fig. 3(a) and Fig. 5(a) are consistent. However, by comparing Fig. 4(a) and Fig. 5(b), it can be seen that the different proportions of indoor and outdoor UEs have impacts on the EEs of the three architectures. The EE are the same for one-link simulations, while the EE is improved by 3.6% without mmWave and by 4.3% with mmWave for two-link simulations. For the one-link network architecture, the different ratio has no impact on EE. Nevertheless, along with the decreasing proportion of indoor UEs, the EE of the two-link architecture shows an obvious decrease, especially for the proposed architecture. The reason is that the two-link architecture with mmWave adopts numerous IAPs to support indoor UEs and the basic power consumption is high. When the number of indoor UEs decreases, the power consumption of IAPs will significantly influence the EE. As a result, Fig. 5(a) and Fig. 5(b) demonstrate that the proposed network architecture is suitable for urban scenarios, such as a city central business district.

In Fig. 6, we compared the total power consumption for different system settings under different data rates. It can be observed that for both the one-link and two-link scenario, when we use more Tx antennas in the MBSA, the system will consume more power, so in the low data rate range, the simpler system will have a better performance in terms of energy consumption. However, in the high data rate range,

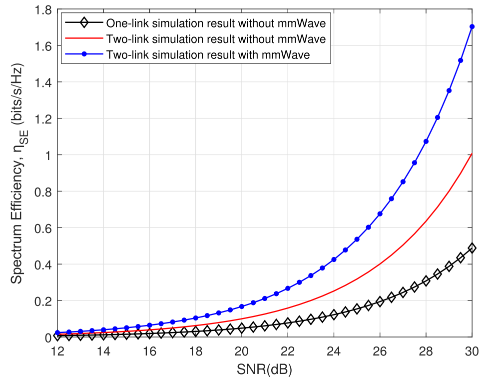

(a) Comparison of SE

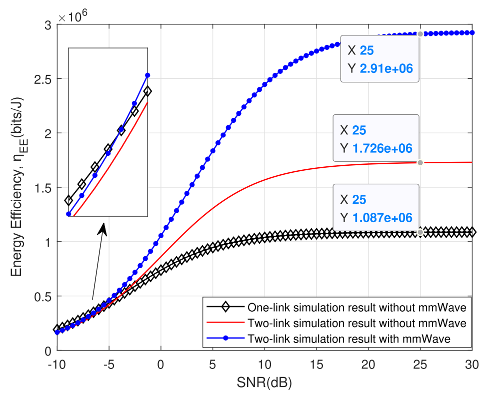

(b) Comparison of EE

Fig. 5. Comparison of SE and EE for one-link and two-link network architectures with and without mmWave technology considering 12 outdoor UEs and 4 indoor UEs.

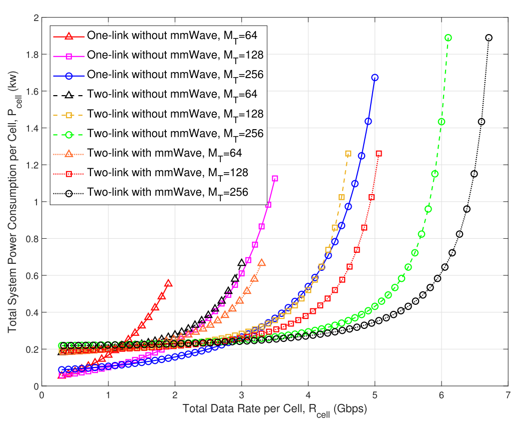

Fig. 6. Comparison of system power consumption at different data rates for one-link and two-link network architectures with and without mmWave technology.

the advantage of more antennas can be observed. A similar observation can be obtained for the two-link mmWave system. Compared with the one-link system with the same Tx antennas, the two-link mmWave system has a worse performance in the low data rate range compared with the one-link solution due to the overheads consumed by the extra components. But in the high data range, the increase in data speed can overcome that extra cost. Based on this observation, we suggest that for the future wireless network, the low data transmission such as the control plane data, conventional one link can be used as the most efficient method, while for the high data rate transmission such as the user plane data, the two-link solution is a better candidate. For future wireless communication system, more dynamic and efficient network management schemes should be designed. Advanced technologies such as the software-defined radio and software-defined networks can be used to allocate resource flexibly, and further improve the system efficiency.

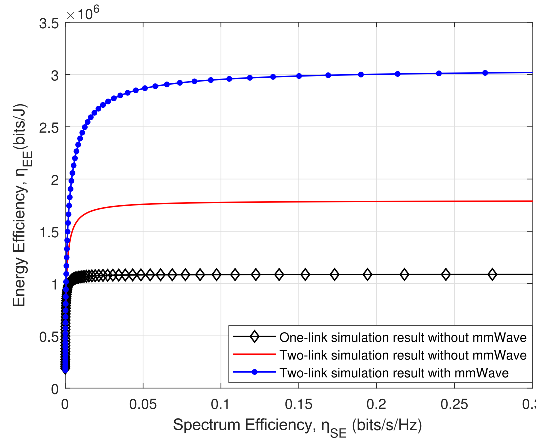

Fig. 7. EE and SE trade-off for one-link and two-link network architectures with and without mmWave technology.

D. Trade-Off Analysis

As shown in [16], in the practical system, when considering the circuit power and others, the SE-EE curve will trun to a bell shape. Hence, it is not always possible to improve both the EE and the SE at the same time. For the optimal performance, the SE versus EE trade-off always need to be considered and the optimization problem can be expressed as

$$\arg \max_{N,\rho} \mathrm{EE}, \ \text{s.t. } \mathrm{SE} = \text{constant} \tag{40}$$

where N denotes the number of users.

The SE versus EE trade-off curves of the three scenarios are shown in Fig. 7. The trends of EE first ascend as SE increases and then remain steady at a certain SE value. It can be observed that with the certain SE, the separated solution could obtain the higher EE, which means that it can achieve a better trade-off for SE and EE as there is no penetration loss. When applying mmWave technology, the system performance is further improved due to a much better interference management. Besides the SE and EE, the economic efficiency metric is also employed to comprehensively evaluate the performance of the system. According to [13], for optimization, the trade-off between ECE, SE, and EE is also needed. The simulation results for the separated and non-separated cases are shown in Figs. 8(a) and 8(b).

In two figures, the trade-off curves both contain the *Pareto-optimal frontier,* representing the efficient operating points. Regardless of whether the separated indoor/outdoor scenarios are adopted, the system can achieve better performance as the number of antennas increases. When the system adopts mmWave, the increase in the number of antennas will significantly enhance the system performance. We observe that the separated mmWave solution with the largest number of

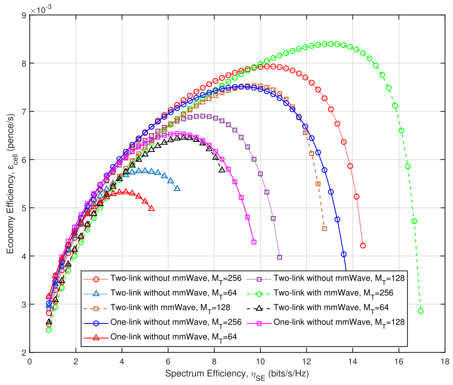

(a) ECE and SE trade-off

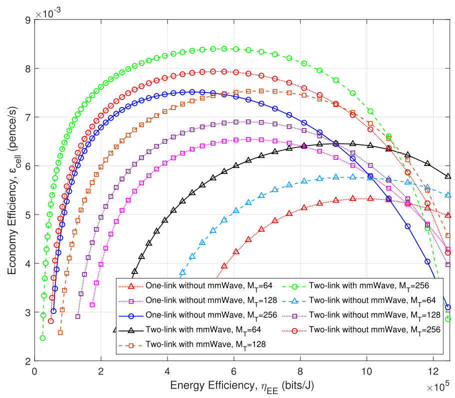

(b) ECE and EE trade-off

Fig. 8. The trade-off between ECE, SE, and EE for one-link and two-link network architectures with and without mmWave technology.

antenna offers the best trade-off in terms of SE, EE, and ECE. That is because a much better SE and EE performance can result in a better revenue efficiency as the unit cost of spectrum and energy for generating data traffic is lower by using this solution. These simulation results indicate that the proposed separated indoor and outdoor solution could potentially be an attractive candidate for the network service providers by offering a balanced trade-off between the system performance and the cost for future wireless communication networks.

V. Conclusion

This paper has investigated the SE, EE, ECE, and analyzed the associated trade-offs for a B5G cellular system with separate outdoor and indoor network deployments. For the outdoor scenario, the MBS is assisted by massive MIMO and DAS technologies at sub-6 GHz frequency bands to serve outdoor UE, and provides access data links for BMAA aided IAPs. In particular, the beamforming technology is applied over the link between the MBSA and the BMAA. For the indoor scenario, IAPs employ mmWave communication and beamforming technologies to serve indoor UE with a high-speed link in a short range. The SE of three types of links has been studied. The power consumption models of the MBSA, the BMAA, and the IAP have been developed considering baseband operations, analog components of the RF front-end, and PAs. The ECE model has been provided with a practical categorization of traffic classes. The basic optimization problem and the simulation results for the trade-offs among SE, EE, ECE have been analyzed. The trade-off curves illustrate that compared with the non-separated system and the separated system without mmWave, the proposed network architecture could obtain the best performance. From the investigation of the SE, EE, ECE and their trade-offs, it can be observed that the proposed cellular architecture is a promising solution for B5G wireless networks deployment.

Appendix

A. Proof of (14)

$$
\begin{aligned}
&\mathbb{E}\left[\left[\sqrt{\beta_{\ell ji} M_R M_T}\sum_{k=1}^{N_{oue}} \mathbf{a}_{MT}^{T}\left(\theta_{\ell ji}\right)\omega_{ki} s_{ki}\right]^2\right]\\
&= \mathbb{E}\left[\left[\sqrt{\beta_{\ell ji} M_R M_T}\sum_{k=1}^{N_{oue}} \frac{1}{\sqrt{M_T}}\right.\right.\\
&\qquad \left.\left.\left[1,\ldots,e^{-j2\pi\Delta(M_T-1)sin\theta_{\ell ji}}\right]\frac{h_{ki}^{*}}{\sqrt{M_T}} s_{ki}\right]^2\right]\\
&= \frac{\beta_{\ell ji} M_R}{M_T}\mathbb{E}\left[\left[\sum_{k=1}^{N_{oue}} h_{ki}^{*} s_{ki}\left[1,\ldots,e^{-j2\pi\Delta(M_T-1)sin\theta_{\ell ji}}\right]\right]^2\right]\\
&= \frac{\beta_{\ell ji} M_R}{M_T}\mathbb{E}\\
&\quad\times\left[\left[\left[\sum_{k=1}^{N_{oue}} h_{ki}^{*} s_{ki},\ldots,\sum_{k=1}^{N_{oue}} h_{ki}^{*} s_{ki} e^{-j2\pi\Delta(M_T-1)sin\theta_{\ell ji}}\right]\right]^2\right]\\
&= \frac{\beta_{\ell ji} M_R}{M_T}\mathbb{E}\left[\left[\sum_{m=1}^{M_T}\sum_{k=1}^{N_{oue}} h_{ki}^{*} s_{ki} e^{-j2\pi\Delta(m-1)sin\theta_{\ell ji}}\right]^2\right]
\end{aligned}
\tag{41}
$$

B. Proof of (15)

$$
\begin{aligned}
&\mathbb{E}\left[\left[\sum_{i'\in\mathcal{N}(i)} \mathbf{a}_{MR}^{T}\left(\phi_{\ell ji}\right)\mathbf{G}_{\ell' j' i'} x_{i'}\right]^2\right]\\
&= \mathbb{E}\left[\left[\sum_{i'\in\mathcal{N}(i)} \mathbf{a}_{MR}^{T}\left(\phi_{\ell ji}\right)\sqrt{\beta_{\ell' j' i'} M_R' M_T'}\right.\right.\\
&\quad \mathbf{a}_{M_R'}^{*}\left(\phi_{\ell' j' i}\right)\mathbf{a}_{M_T'}^{T}\left(\theta_{\ell' j' i}\right)\\
&\quad \left.\left.\left(\sum_{j=1}^{N_b}\sum_{l=1}^{L}\mathbf{b}_{\ell' j' i} s_{\ell' j' i} + \sum_{k=1}^{N_{oue}} \omega_{ki'} s_{ki'}\right)\right]^2\right]\\
&= \beta_{\ell' j' i'} M_R' M_T' \mathbb{E}\left[\left[\sum_{i'\in\mathcal{N}(i)}\left[\mathbf{a}_{MR}^{T}\left(\phi_{\ell ji}\right)\mathbf{a}_{M_R'}^{*}\left(\phi_{\ell' j' i}\right) s_{\ell' j' i}\right.\right.\right.\\
&\quad \left.\left.\left. +\mathbf{a}_{MR}^{T}\left(\phi_{\ell ji}\right)\mathbf{a}_{M_R'}^{*}\left(\phi_{\ell' j' i}\right)\sum_{k=1}^{N_{oue}}\mathbf{a}_{M_T'}^{T}\left(\theta_{\ell' j' i}\right)\omega_{ki'} s_{ki'}\right]\right]^2\right].
\end{aligned}
\tag{42}
$$

It is reasonable to assume that receivers have the same number of receiving antennas, i.e., $M_R' = M_R$. Based on the assumption, (15) can be obtained.

References

[1] C.-X. Wang et al., "On the road to 6G: Visions, requirements, key technologies and testbeds," *IEEE Commun. Surveys Tuts.*, early access, Feb. 27, 2023, doi: 10.1109/COMST.2023.3249835.

[2] C.-X. Wang, Z. Lv, X. Gao, X. You, Y. Hao, and H. Haas, "Pervasive wireless channel modeling theory and applications to 6G GBSMs for all frequency bands and all scenarios," *IEEE Trans. Veh. Technol.*, vol. 71, no. 9, pp. 9159–9173, Sep. 2022.

[3] R. Borralho, A. Mohamed, A. U. Quddus, P. Vieira, and R. Tafazolli, "A survey on coverage enhancement in cellular networks: Challenges and solutions for future deployments," *IEEE Commun. Surveys Tuts.*, vol. 23, no. 2, pp. 1302–1341, 2nd Quart., 2021.

[4] E. G. Larsson, O. Edfors, F. Tufvesson, and T. L. Marzetta, "Massive MIMO for next generation wireless systems," *IEEE Commun. Mag.*, vol. 52, no. 2, pp. 186–195, Feb. 2014.

[5] C.-X. Wang, J. Bian, J. Sun, W. Zhang, and M. Zhang, "A survey of 5G channel measurements and models," *IEEE Commun. Surveys Tuts.*, vol. 20, no. 4, pp. 3142–3168, 4th Quart., 2018.

[6] J. Wang et al., "A novel 3D non-stationary GBSM for 6G THz ultra-massive MIMO wireless systems," *IEEE Trans. Veh. Technol.*, vol. 70, no. 12, pp. 12312–12324, Dec. 2021.

[7] L. Lu, G. Y. Li, A. L. Swindlehurst, A. Ashikhmin, and R. Zhang, "An overview of massive MIMO: Benefits and challenges," *IEEE J. Sel. Topics Signal Process.*, vol. 8, no. 5, pp. 742–758, Oct. 2014.

[8] J. Huang, C.-X. Wang, R. Feng, J. Sun, W. Zhang, and Y. Yang, "Multi-frequency mmWave massive MIMO channel measurements and characterization for 5G wireless communication systems," *IEEE J. Sel. Areas Commun.*, vol. 35, no. 7, pp. 1591–1605, Jul. 2017.

[9] J. Huang, C.-X. Wang, Y. Liu, J. Sun, and W. Zhang, "A novel 3D GBSM for mmWave MIMO channels," *Sci. China Inf. Sci.*, vol. 61, no. 10, pp. 1–15, Oct. 2018.

[10] W. Roh et al., "Millimeter-wave beamforming as an enabling technology for 5G cellular communications: Theoretical feasibility and prototype results," *IEEE Commun. Mag.*, vol. 52, no. 2, pp. 106–113, Feb. 2014.

[11] A. Chowdhury, P. Sasmal, C. R. Murthy, and R. Chopra, "On the performance of distributed antenna array systems with quasi-orthogonal pilots," *IEEE Trans. Veh. Technol.*, vol. 71, no. 3, pp. 3326–3331, Mar. 2022.

[12] I. Ku, C.-X. Wang, and J. Thompson, "Spectral-energy efficiency tradeoff in relay-aided cellular networks," *IEEE Trans. Wireless Commun.*, vol. 12, no. 10, pp. 4970–4982, Oct. 2013.

[13] I. Ku, C.-X. Wang, and J. S. Thompson, "Spectral, energy and economic efficiency of relay-aided cellular networks," *IET Commun.*, vol. 7, no. 14, pp. 1476–1487, Sep. 2013.

[14] H. A. Ammar, R. Adve, S. Shahbazpanahi, G. Boudreau, and K. V. Srinivas, "User-centric cell-free massive MIMO networks: A survey of opportunities, challenges and solutions," *IEEE Commun. Surveys Tuts.*, vol. 24, no. 1, pp. 611–652, 1st Quart., 2022.

[15] C.-X. Wang et al., "Cellular architecture and key technologies for 5G wireless communication networks," *IEEE Commun. Mag.*, vol. 52, no. 2, pp. 122–130, Feb. 2014.

[16] Y. Chen et al., "Fundamental trade-offs on green wireless networks," *IEEE Commun. Mag.*, vol. 49, no. 6, pp. 30–37, Jun. 2011.

[17] C. He, B. Sheng, P. Zhu, and X. You, "Energy efficiency and spectral efficiency tradeoff in downlink distributed antenna systems," *IEEE Wireless Commun. Lett.*, vol. 1, no. 3, pp. 153–156, Jun. 2012.

[18] B. D. Antwi-Boasiako, R. K. Ahiadormey, P. Anokye, and K.-J. Lee, "On the performance of massive MIMO full-duplex relaying with low-resolution ADCs," *IEEE Commun. Lett.*, vol. 26, no. 6, pp. 1259–1263, Jun. 2022.

[19] Y. Huang, S. He, J. Wang, and J. Zhu, "Spectral and energy efficiency tradeoff for massive MIMO," *IEEE Trans. Veh. Technol.*, vol. 67, no. 8, pp. 6991–7002, Aug. 2018.

[20] V. H. Nguyen et al., "On the spectral and energy efficiencies of full-duplex cell-free massive MIMO," *IEEE J. Sel. Areas Commun.*, vol. 38, no. 8, pp. 1698–1718, Aug. 2020.

[21] O. Amin, E. Bedeer, M. H. Ahmed, and O. A. Dobre, "Energy efficiency-spectral efficiency trade-off: A multi objective optimization approach," *IEEE Trans. Veh. Technol.*, vol. 65, no. 4, pp. 1975–1981, Apr. 2016.

[22] H. Q. Ngo, E. G. Larsson, and T. L. Marzetta, "Energy and spectral efficiency of very large multiuser MIMO systems," *IEEE Trans. Commun.*, vol. 61, no. 4, pp. 1436–1449, Apr. 2013.

[23] A. Salem, L. Musavian, and K. A. Hamdi, "Wireless power transfer in distributed antenna systems," *IEEE Trans. Commun.*, vol. 67, no. 1, pp. 737–747, Jan. 2019.

[24] Z. Chen, T. Q. S. Quek, and Y.-C. Liang, "Spectral efficiency and relay energy efficiency of full-duplex relay channel," *IEEE Trans. Wireless Commun.*, vol. 16, no. 5, pp. 3162–3175, May 2017.

[25] E. Sharma, A. K. Shukla, and R. Budhiraja, "Spectral- and energy-efficiency of massive MIMO two-way half-duplex hybrid processing AF relay," *IEEE Wireless Commun. Lett.*, vol. 7, no. 5, pp. 876–879, Oct. 2018.

[26] S. K. Mohammed, "Impact of transceiver power consumption on the energy efficiency of zero-forcing detector in massive MIMO systems," *IEEE Trans. Commun.*, vol. 62, no. 11, pp. 3874–3890, Nov. 2014.

[27] J. Qian, C. Masouros, and M. Matthaiou, "Multi-pair two-way massive MIMO relaying with zero forcing: Energy efficiency and power scaling laws," *IEEE Trans. Commun.*, vol. 68, no. 3, pp. 1417–1431, Mar. 2020.

[28] Y. Zhang, Y. Xu, Y. Sun, Q. Wu, and K. Yao, "Energy efficiency of small cell networks: Metrics, methods and market," *IEEE Access*, vol. 5, pp. 5965–5971, 2017.

[29] Y. Zhang, M. Xiao, S. Han, M. Skoglund, and W. Meng, "On precoding and energy efficiency of full-duplex millimeter-wave relays," *IEEE Trans. Wireless Commun.*, vol. 18, no. 3, pp. 1943–1956, Mar. 2019.

[30] Y. Fu et al., "End-to-end energy efficiency evaluation for B5G ultra dense networks," in *Proc. IEEE 91st Veh. Technol. Conf. (VTC-Spring)*, Antwerp, Belgium, May 2020, pp. 1–6.

[31] P. Patcharamaneepakorn et al., "Spectral, energy, and economic efficiency of 5G multicell massive MIMO systems with generalized spatial modulation," *IEEE Trans. Veh. Technol.*, vol. 65, no. 12, pp. 9715–9731, Dec. 2016.

[32] M. K. Mishra and A. Trivedi, "Spectral efficiency and deployment cost efficiency analysis of mmW/UHF-based cellular network," *IEEE Trans. Veh. Technol.*, vol. 68, no. 7, pp. 6565–6577, Jul. 2019.

[33] C. Li, J. Zhang, and K. B. Letaief, "Throughput and energy efficiency analysis of small cell networks with multi-antenna base stations," *IEEE Trans. Wireless Commun.*, vol. 13, no. 5, pp. 2505–2517, May 2014.

[34] J. Ghosh, "A trade-off between energy efficiency and spectral efficiency in macro-femtocell networks," *IEEE Trans. Veh. Technol.*, vol. 69, no. 10, pp. 10914–10924, Oct. 2020.

[35] Z. Zhang, Z. Chen, M. Shen, and B. Xia, "Spectral and energy efficiency of multipair two-way full-duplex relay systems with massive MIMO," *IEEE J. Sel. Areas Commun.*, vol. 34, no. 4, pp. 848–863, Apr. 2016.

[36] H. Belay, K. Kornegay, and E. Ceesay, "Energy efficiency analysis of RLS-MUSIC based smart antenna system for 5G network," in *Proc. 55th Annu. Conf. Inf. Sci. Syst. (CISS)*, Baltimore, MD, USA, Mar. 2021, pp. 1–5.

[37] S. Bhattacharyya and G. Aruna, "Radiation pattern analysis of uniform rectangular planar arrays for millimeter wave communications: Comparative study with uniform linear arrays," *Wireless Pers. Commun.*, vol. 112, no. 2, pp. 827–848, May 2020.

[38] V. P. Selvan, M. S. Iqbal, and H. S. Al-Raweshidy, "Performance analysis of linear precoding schemes for very large multi-user MIMO downlink system," in *Proc. INTECH*, Luton, U.K., Aug. 2014, pp. 219–224.

[39] Q. Zhang, S. Jin, K. K. Wong, H. Zhu, and M. Matthaiou, "Power scaling of uplink massive MIMO systems with arbitrary-rank channel means," *IEEE J. Sel. Topics Signal Process.*, vol. 8, no. 5, pp. 966–981, May 2014.

[40] G. Auer et al., "How much energy is needed to run a wireless network?" *IEEE Trans. Wireless Commun.*, vol. 18, no. 5, pp. 40–49, Oct. 2011.

[41] C. Desset, P. Wambacq, Y. Zhang, M. Ingels, and A. Bourdoux, "A flexible power model for mm-wave and THz high-throughput communication systems," in *Proc. IEEE 31st Annu. Int. Symp. Pers., Indoor Mobile Radio Commun.*, London, U.K., Aug. 2020, pp. 1–6.

[42] W. Liu, S. Han, and C. Yang, "Energy efficiency scaling law of massive MIMO systems," *IEEE Trans. Commun.*, vol. 65, no. 1, pp. 107–121, Jan. 2017.

[43] C. Desset, B. Debaillie, and F. Louagie, "Modeling the hardware power consumption of large scale antenna systems," in *Proc. IEEE Online Conf. Green Commun. (OnlineGreenComm)*, Tucson, AZ, USA, Nov. 2014, pp. 1–6.

[44] C. Desset et al., "Flexible power modeling of LTE base stations," in *Proc. IEEE Wireless Commun. Netw. Conf. (WCNC)*, Paris, France, Apr. 2012, pp. 2858–2862.

[45] P. Kyosti. (Sep. 2007). *IST-4-027756 WINNER II D1.1.2 WINNER II Channel Models*. [Online]. Available: https://www.istwinner.org/WINNER2-Deliverables/D1.1.2v1.1.pdf

[46] S. Deng, M. K. Samimi, and T. S. Rappaport, "28 GHz and 73 GHz millimeter-wave indoor propagation measurements and path loss models," in *Proc. IEEE Int. Conf. Commun. Workshop (ICCW)*, London, U.K., Jun. 2015, pp. 1244–1250.

[47] H. Holma and A. Toskala, *WCDMA for UMTS: HSPA Evolution and LTE*, 5th ed. Hoboken, NJ, USA: Wiley, 2010.

[48] C. Lin and G. Y. Li, "Energy-efficient design of indoor mmWave and sub-THz systems with antenna arrays," *IEEE Trans. Wireless Commun.*, vol. 15, no. 7, pp. 4660–4672, Mar. 2016.

Yu Fu received the B.Sc. degree in computer science from Huaqiao University, Fujian, China, in 2009, and the M.Sc. degree in information technology (mobile communications) and the Ph.D. degree in wireless communications from Heriot-Watt University, Edinburgh, U.K., in 2010 and 2015, respectively. He has been a Post-Doctoral Research Associate with Heriot-Watt University, since 2015. His main research interests include advanced MIMO communication technologies, wireless channel modeling and simulation, RF tests, and software defined networks.

Cheng-Xiang Wang (Fellow, IEEE) received the B.Sc. and M.Eng. degrees in communication and information systems from Shandong University, China, in 1997 and 2000, respectively, and the Ph.D. degree in wireless communications from Aalborg University, Denmark, in 2004.

He was a Research Assistant with the Hamburg University of Technology, Hamburg, Germany, from 2000 to 2001; a Visiting Researcher with Siemens AG Mobile Phones, Munich, Germany, in 2004; and a Research Fellow with the University of Agder, Grimstad, Norway, from 2001 to 2005. He has been with Heriot-Watt University, Edinburgh, U.K., since 2005, where he was promoted to a Professor in 2011. In 2018, he joined Southeast University, Nanjing, China, as a Professor. He is also a part-time Professor with the Purple Mountain Laboratories, Nanjing. He has authored four books, three book chapters, and more than 500 papers in refereed journals and conference proceedings, including 27 highly cited papers. He has also delivered 24 invited keynote speeches/talks and 16 tutorials in international conferences. His current research interests include wireless channel measurements and modeling, 6G wireless communication networks, and electromagnetic information theory.

Dr. Wang is a member of the Academia Europaea (The Academy of Europe) and the European Academy of Sciences and Arts (EASA); and a fellow of the Royal Society of Edinburgh (FRSE), IET, and the China Institute of Communications (CIC). He received 15 Best Paper Awards from IEEE GLOBECOM 2010, IEEE ICCT 2011, ITST 2012, IEEE VTC 2013 Spring, IWCMC 2015, IWCMC 2016, IEEE/CIC ICCC 2016, WPMC 2016, WOCC 2019, IWCMC 2020, WCSP 2020, CSPS2021, WCSP 2021, and IEEE/CIC ICCC 2022. He has served as a TPC member, the TPC chair, and the general chair for more than 30 international conferences. He is currently an Executive Editorial Committee Member of the IEEE Transactions on Wireless Communications. He has served as an Editor for over ten international journals, including the IEEE Transactions on Wireless Communications, from 2007 to 2009, the IEEE Transactions on Vehicular Technology, from 2011 to 2017, and the IEEE Transactions on Communications, from 2015 to 2017. He was a Guest Editor of the IEEE Journal on Selected Areas in Communications, Special Issue on Vehicular Communications and Networks (a Lead Guest Editor), Special Issue on Spectrum and Energy Efficient Design of Wireless Communication Networks, and Special Issue on Airborne Communication Networks. He was also a Guest Editor of the IEEE Transactions on Big Data, Special Issue on Wireless Big Data. He is a Guest Editor of the IEEE Transactions on Cognitive Communications and Networking, Special Issue on Intelligent Resource Management for 5G and Beyond. He is an IEEE Communications Society Distinguished Lecturer, from 2019 to 2020, and a Highly-Cited Researcher recognized by Clarivate Analytics in 2017 and 2020.

Xichen Mao received the B.E. degree in communication engineering from Jilin University, China, in 2021. He is currently pursuing the Ph.D. degree with the National Mobile Communications Research Laboratory, Southeast University, China. His research interests include 6G communication performance analysis and system optimization.

Jie Huang (Member, IEEE) received the B.E. degree in information engineering from Xidian University, China, in 2013, and the Ph.D. degree in information and communication engineering from Shandong University, China, in 2018. From October 2018 to October 2020, he was a Post-Doctoral Research Associate with the National Mobile Communications Research Laboratory, Southeast University, China, supported by the National Post-Doctoral Program for Innovative Talents. From January 2019 to February 2020, he was a Post-Doctoral Research Associate with Durham University, U.K. Since March 2019, he has been a part-time Researcher with the Purple Mountain Laboratories, China. Since November 2020, he has been an Associate Professor with the National Mobile Communications Research Laboratory, Southeast University. He has authored or coauthored more than 70 papers in refereed journals and conference proceedings. His research interests include millimeter wave, massive MIMO, reconfigurable intelligent surface channel measurements and modeling, wireless big data, and 6G wireless communications. He received the Best Paper Awards from WPMC 2016, WCSP 2020, and WCSP 2021. He has delivered nine tutorials in IEEE/CIC ICCC 2021, IEEE PIMRC 2021, IEEE ICC 2022, IEEE VTC-Spring 2022, IEEE/CIC ICCC 2022, IEEE VTC-Fall 2022, IEEE PIMRC 2022, IEEE Globecom 2022, and IEEE WCNC 2023.

Zijun Zhao received the B.Eng. degree from the School of Information Science and Engineering, Shandong University, Jinan, China, in 2018, and the M.S. degree in electrical engineering from Columbia University, New York, NY, USA, in 2020. She is currently a Communications Systems Engineer with Huawei Technologies Company Ltd., Shanghai, China. Her research interests include green networking and radio resource management of base stations.

Stephen McLaughlin (Fellow, IEEE) received the B.Sc. degree from the University of Glasgow, Glasgow, U.K., in 1981, and the Ph.D. degree from The University of Edinburgh, Edinburgh, U.K., in 1990. From 1981 to 1986, he was a development engineer in industry. In 1986, he joined the Department of Electronics and Electrical Engineering, The University of Edinburgh, as the Chair of electronic communication systems. In October 2011, he joined Heriot-Watt University, Edinburgh, as a Professor of signal processing. He is a fellow of the Royal Academy of Engineering, the Royal Society of Edinburgh, and the Institute of Engineering and Technology. He is also a EURASIP Fellow.